Journal of Seismology 5: 63–72, 2001.

Semi-empirical estimation of ground motion using observed records at a site in Shikoku, Japan

Yoshimitsu Fukushima[1], Masafumi Mori[1], Shin'ichi Matsuzaki[2], Shuji Kobayashi[2] & Yuki Ohno[2]

[1] *Ohsaki Research Institute, Tokyo, Japan;* [2] *Shikoku Electric Power Company, Takamatsu, Japan*

Received 2 September 1998; accepted in revised form 14 December 1999

Key words: asperity, empirical Green's function, fault plane, inhomogeneous fault, median tectonic line, response spectra, semi-empirical method, strong ground motion

Abstract

A semi-empirical approach using fore- or after-shock records as Green's functions is applicable to the simulation of strong ground motion, however such records are obviously not available for prediction purposes. Thus we have predicted ground motion for a hypothetical large earthquake from other minor events by adopting a distance correction based on geometrical spreading. Another difficulty in prediction is fault modeling. Surface traces were simplified as fault models 27, 46, 55, and 77 km in length. Further, the actual fault rupture may be inhomogeneous, so an asperity distribution is assumed. This asperity model assumes that dislocation and stress drop are double than the average values. Although, the near field term is neglected in our simulation, no significant difference was seen in the motions estimated by individual models for periods up to 2.0 seconds. This indicates that the dependence of source size is small for strong motion, perhaps as a result of the random summation of high-frequency phases.

Introduction

Since the 1995 Hyogo-ken Nanbu earthquake, the importance of estimating strong ground motion near a fault has been more keenly recognized. The methods of carrying out such estimations depend on theoretical, empirical, or semi-empirical approaches. Theoretical methods such as the dislocation theory are physically meaningful, but it is very difficult to generate the higher-frequency components above 1.0 Hz that have a significant effect on stiff structures. On the other hand, an empirical approach (Kobayashi and Midorikawa, 1982) provides estimates of the high-frequency component, but has less physical meaning. A semi-empirical approach using a small event record as a Green's function (Dan et al., 1990a) is a very useful technique for obtaining the high-frequency component, as long as fore- or after-shock records are available. A limit preventing use of the method to near-sources areas exists (Bour and Cara, 1997), but Kamae and Irikura (1998) succeeded in simulating the strong motion with a predominant period up to 5 seconds at the Kobe University site, from where the closest distance to the fault of the 1995 Hyogo-ken Nanbu earthquake may be less than 2 km. The difficulty with this method of prediction is obtaining such records for the site of interest. However, rather than fore- or after-shocks, it is possible to obtain records of weak motion. Site and path effects would be included in these records. Further, the source location of such small events can be corrected by geometrical spreading. Although the seismological information acquired is very limited, we attempt to simulate strong motion from hypothetical large faults by the semi-empirical Green's function method using corrected small records as Green's functions.

Site

The site is located on the north shore of the Sadamisaki peninsula, at the western tip of Japan's Shikoku Island. There is a nuclear power plant in the vicinity, so estimation of higher-frequency input ground mo-

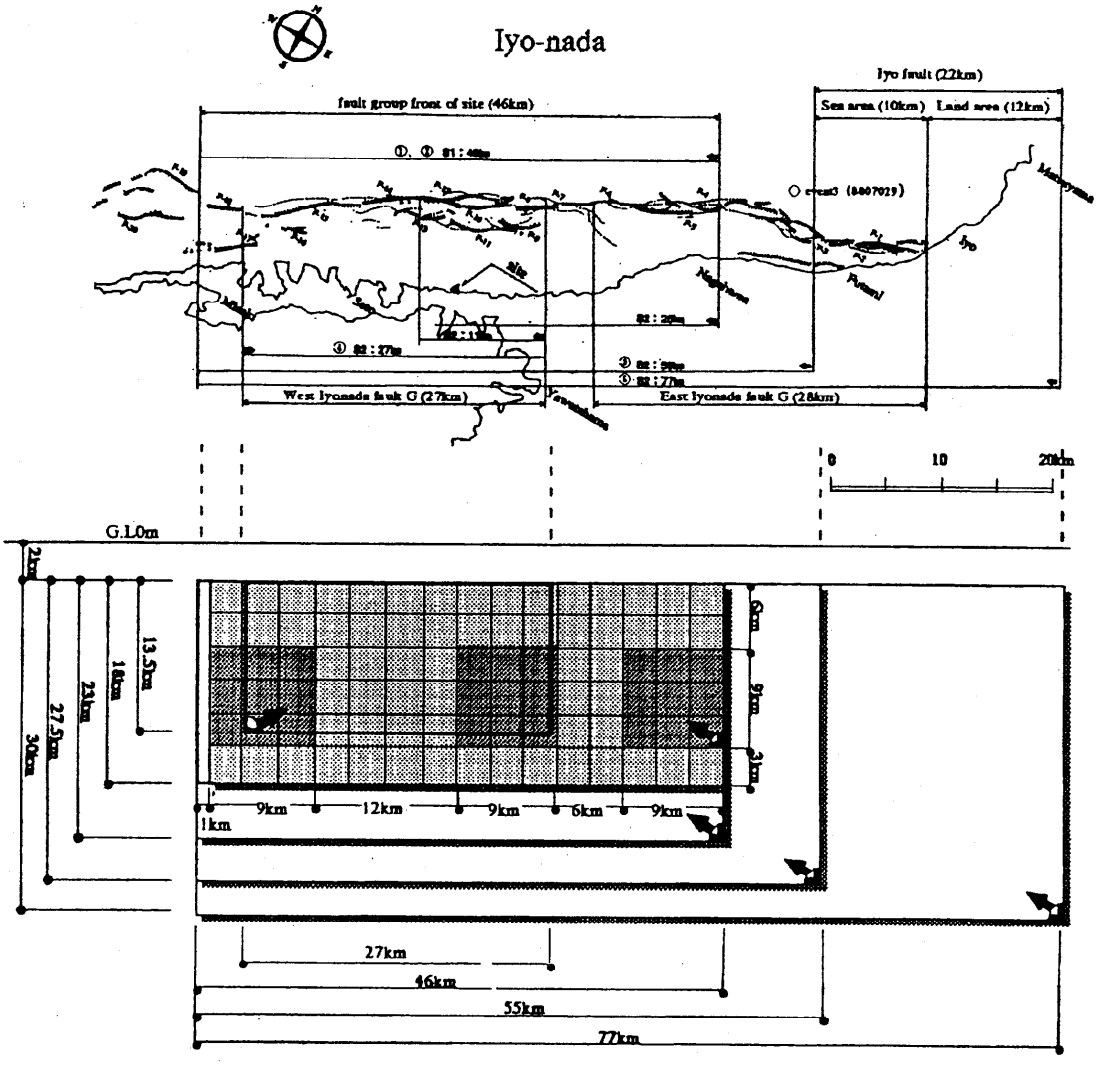

Figure 1. Location of fault traces, site, and epicenter of small event. Section indicates fault models for 27, 46, 55, and 77 km, as well as the asperity model. Arrows indicate rupture initiation points.

tion with a frequency above 0.5 Hz is very important for safety. The Median tectonic line runs east to west across the island. Lineaments parallel to this line were found off the coast of the site by sonic exploration (Ohno et al., 1998). Some of these are Quaternary active faults. An accerelometer was installed at a depth of 5 m in green schist of the Sanbagawa belt. The S-wave velocity of the schist was found to be 2.6 km/s by PS well-log interpretation. Although the rock near the surface is weathered, it is assumed that the sensor settled on a rock outcrop. The site location and nearby lineaments are shown in Figure 1. The closest distance from the site to a fault is about 8 km. Bour and Cara (1997) demonstrated that the empirical Green's function technique is not applicable in the near field, specially for long period, due to the effect of the near-field term. Also the largest effect of the intermediate- to far-field term can be described as 11 $\beta/3r\omega$ (Dan et al., 1990b), where β is the S-wave velocity, r is the closest distance to the fault, and ω is circular frequency. If β = 3 km/s and r = 8 km are assumed, the contribution of the intermediate terms ranges from 1% to 43% for the predominant period from 0.05 to 2.0 seconds, which is our objective period range. The contribution of the near-field term to the far-field could not be solved as that of the intermediate term. Dan et al. (1987) and Dan and Sato (1998) demonstrated that near-source records from a station located at the

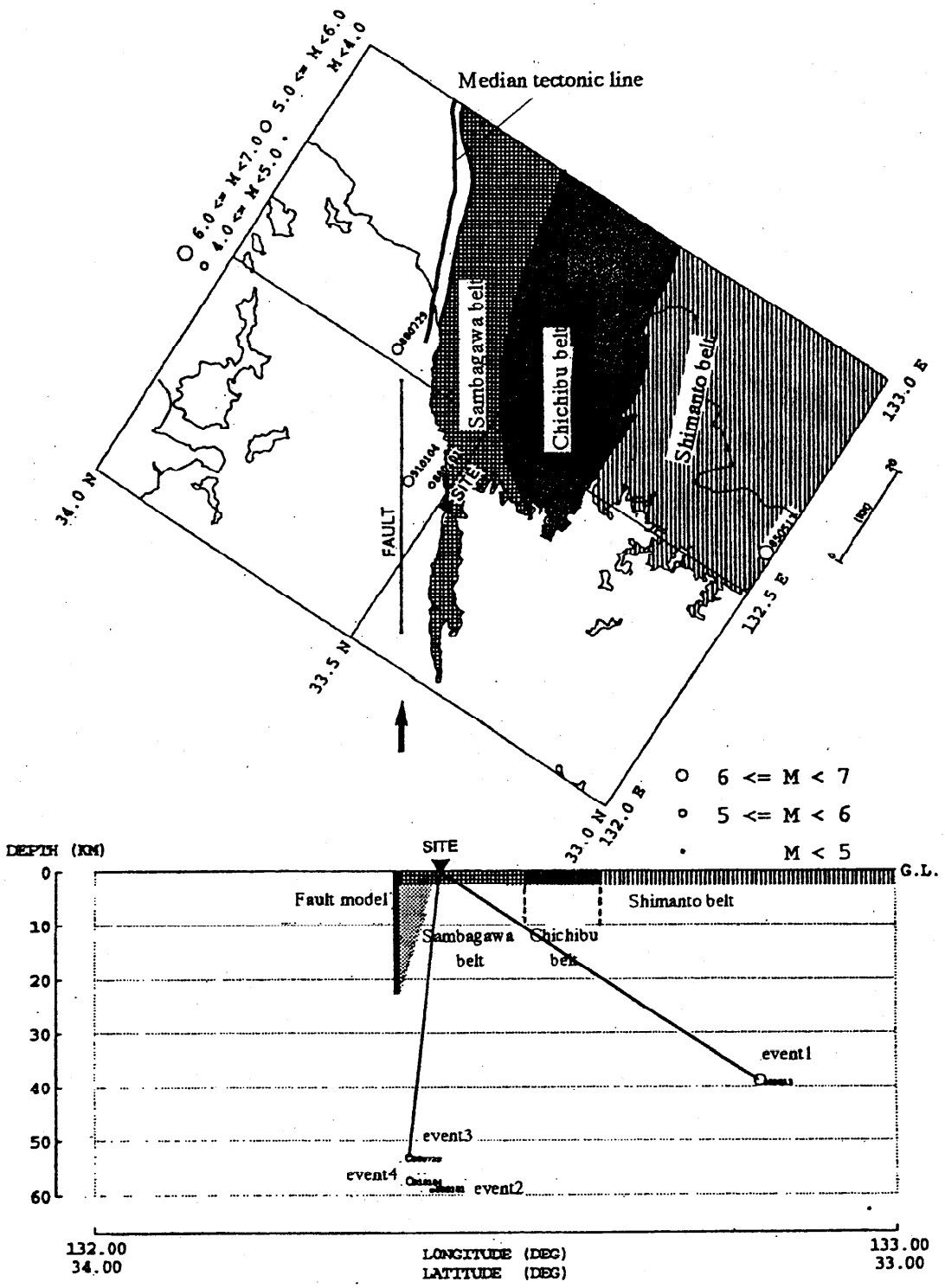

Figure 2. Schematic map and section of tectonic unit around western Shikoku and event epicenters.

closest distance to the fault of less than 4 km could not be simulated for the 1979 Imperial valley, California, earthquake. However, they also demonstrated that the strong motion records from a distance of over 4 km are well simulated by the constant-slip rupture model (Dan et al., 1987) and also by the variable-slip rupture model (Dan and Sato, 1998). Although our site is located 8 km away from the fault, affect of the near-field term may still remain for larger events than the 1979 Imperial Valley earthquake (*M*w 6.5).

Data

As shown in Table 1, records from only four events could be selected as Green's functions due to their proximity and large peak accelerations. The location of these events, the site, approximate fault, and geology are shown in Figure 2. The events used as Green's function should ideally be located on the fault model, but unfortunately the area around our site is one of low seismicity and the events did not occur on the fault plane. The focal depth of these events was relatively deeper than the fault model. The crustal structure in this area may not be homogeneous, but we have little information on this subject, Moreover, simple geometrical spreading can be assumed for near distances in the case of small events (Dieterich, 1973), so event locations are normalized onto the fault plane by a simple distance correction based on a geometrical spreading of 1/R, where R is the distance from source to site. Long period noise contaminates the records in the case of events 2 and 4 in the period range of less than two seconds. Further, event 2 is smaller than *M* 5.0, so it was rejected. On the other hand, event 1 is of large magnitude but was distant from the site, and the ray path of the event crosses three geological belts. For these reasons, the records of event 3 are the most suitable to use as the Green's function, and these records are shown in Figure 3. Further, as shown in the section of Figure 2, most rays from the event probably pass along the assumed fault plane.

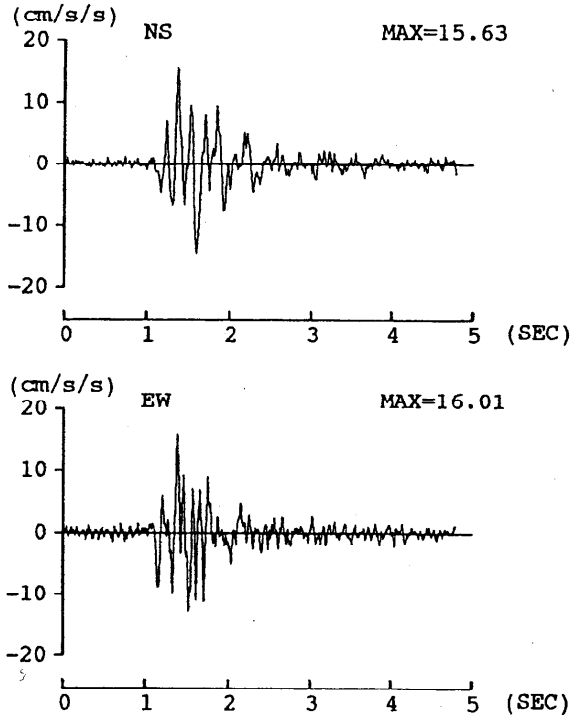

Figure 3. Record of small event 3.

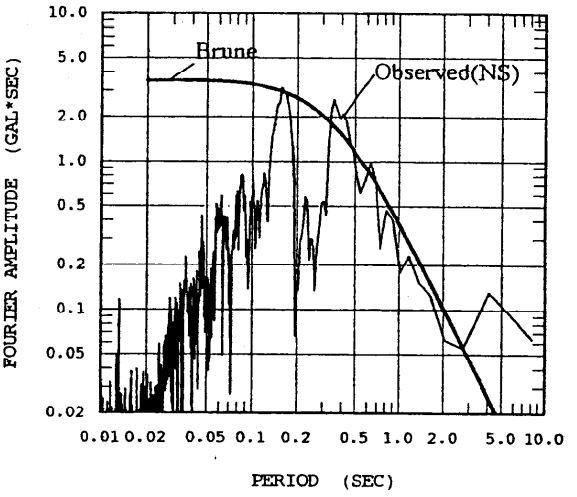

Figure 4. Comparison between Fourier amplitude of observed record and Brune model.

Method

The spatial and temporal aliasing of empirical Green's function techniques has prevented application of the techniques for engineering purpose. However, there is no temporal aliasing in Dan et al. (1990a) as a result of frequency domain synthesis (Zhao et al., 1995). Spatial aliasing is considerable, if small elements are arranged in an identical spacing and the site is located almost equivalent radiation azimuth from the elements (Bour and Cara, 1997). However, in order to eliminate spatial aliasing, rupture points are randomly located in the small elements after Dan et al. (1993) (Zhao et al., 1996).

Table I. Origin of recorded event and peak acceleration

No.	Year/month/day	Lat.	Long.	M	depth.	epicentral distance	PGA
		(N)	(E)		(km)	(km)	(cm/s/s)
1	1985/05/13	32.995	132.587	6.0	39	60	23
2	1988/01/01	33.51	132.34	4.7	59	4	20
3	1988/07/29	33.678	132.508	5.1	53	28	16
4	1991/01/04	33.545	132.322	5.1	58	7	34

First, based on scaling by the ω^{-2} model, the dislocation and stress drop of small events are corrected to those of large events in the frequency domain. As a result of the dislocation correction, longer period component of records than the corner period is according to those of the large event. The seismic moment and stress drop has not been systematically determined for such small events, so they were determined by comparison between theoretical (Brune, 1970) and observed Fourier amplitudes, as shown in Figure 4. The theoretical amplitude well corresponds with the observed amplitude for periods longer than 0.15 second. Although rough estimations are based on the observed record only. the derived moment and stress drop of the small event are 5.63×10^{22} dyne*cm and 200 bar, respectively. The ratios of fault length, width, and dislocation between the small and large events are the cube root of the seismic moment ratio:

$$L_L/L_S = W_L/W_S = D_L/D_S = n,$$
$$Mo_L/Mo_S = n^3 \quad (1)$$

Where L, W, D, and Mo are the length, width, dislocation, and moment, and the suffices L and S indicate the large and small events. Bour and Cara (1997) note that in the case of large magnitude, from 7 to 8, crustal earthquakes, equation (1) no longer holds. Therefore, W and D are estimated in the case of an inhomogeneous model independently on the scaling of equation (1).

Second, the small events are arranged geometrically on the assumed fault model corresponding to ratio n. Then these corrected records are synthesized with an arrival time delay to compensate for the rupture propagation process of the large event, and also considering the geometrical spreading from the elements to the site. The seismic moment derived in the first step is, however, too small to allow deduction of spacial aliasing, namely the ghost noise due to spacial periodicity such as Bour and Cara (1997). Therefore, we synthesize a middle-sized event of 5^3 or 3^3 times the small event, assuming a radial rupture. Namely, the moment of the Green's function is increased to 7.04 or 1.52×10^{24} dyne*cm and used as the Green's function for a homogeneous or inhomogeneous fault model. The radiation pattern is unknown for small events, but it is certainly too complicated to correct in practice, especially at short periods, due to multiple-path effects (Liu and Helmberger, 1985; Somerville et al., 1991). Moreover, coherence of radiation pattern from the each element is small, because the azimuth from individual elements to the site is not constant in our simulation, therefore, no correction of the patterns is applied in this study.

Assumed fault model

Homogeneous faults

As shown in Figure 1, we assumed fault models of length of 27, 46, 55, and 77 km, having widths equal to half the length. The dislocations are assumed to be 210, 363, 420, and 630 cm based on an empirical relation (Matsuda, 1975). Strike and dip angles are 57 and 90 degrees. The models have an assumed depth of 2 km. Rigidity μ and S-wave velocity are 4.0×10^{11} dyne/cm^2 and 3.5 km/s, respectively. Thus, the seismic moments for the individual models are 0.31, 1.52, 2.54, and 5.82×10^{27}dyne*cm. Taking event 3 as the Green's function, the factor n for the 27, 46, 55, and 77 km models is 4, 6, 7, and 10, respectively. The stress drop is assumed to be 50 bar, which is the average in Japan (Sato, 1989). As shown in Figure 1, the rupture initiation points are conservatively assumed to be at the deepest point at the western end in the case of the 27 km model, and otherwise at the eastern end.

Inhomogeneous fault

Recently, inhomogeneitiy of slip distribution has been revealed in the case of some large events (Wald, 1996).

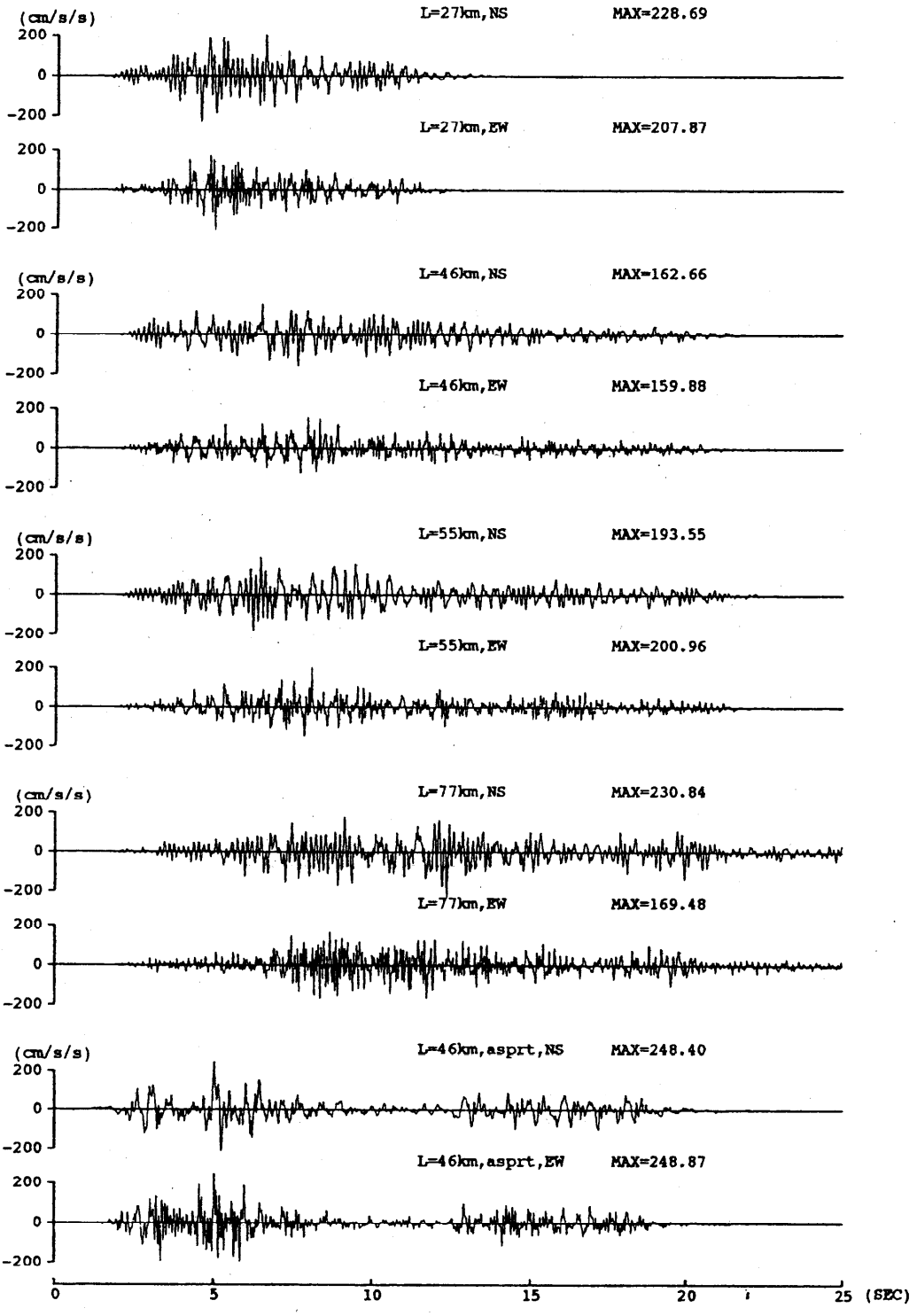

Figure 5. Synthesized waves for fault model lengths of 27, 46, 55, and 77 km, as well as the asperity model.

Table 2. Peak ground accelerations of synthesized waves

Model	Homogeneous				Asperity
Fault length	27 km	46 km	55 km	77 km	46 km
NS (cm/s/s)	229	163	194	231	248
EW (cm/s/s)	208	160	201	169	249

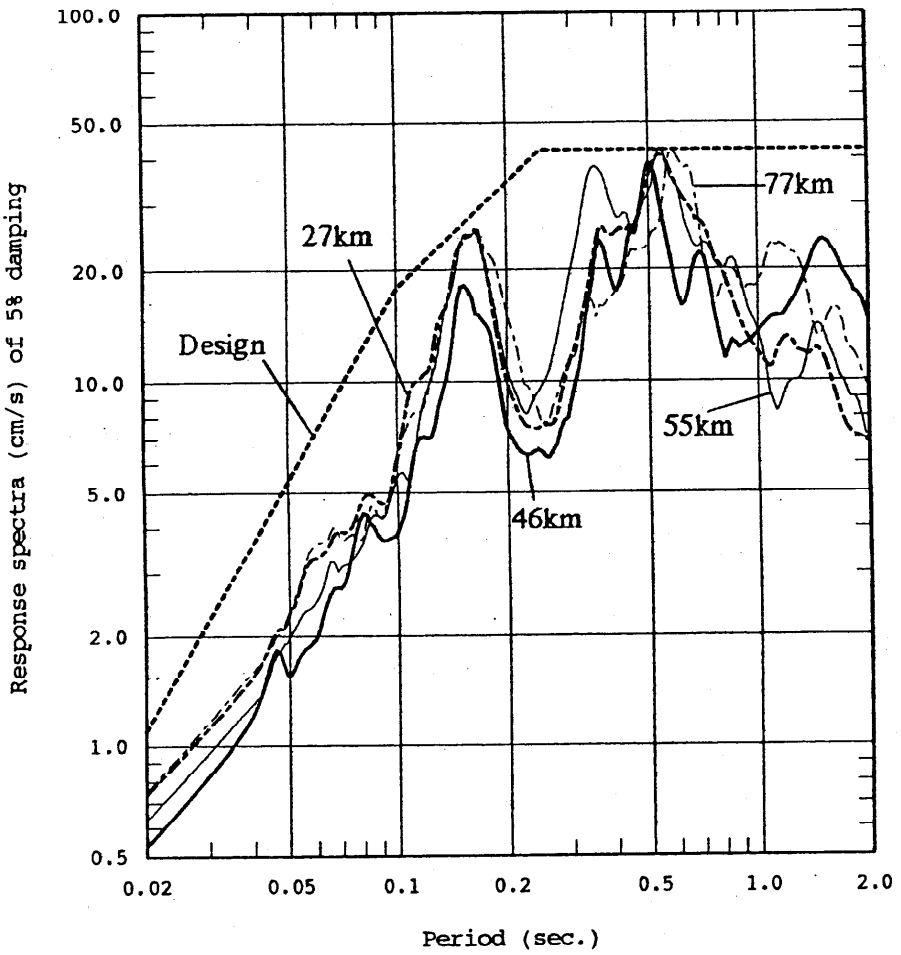

Figure 6. Pseudo velocity response spectra of 5% damping of NS component for fault model lengths of 27, 46, 55, and 77 km, as well as design spectrum.

Somerville et al. (1993) defined 'asperity' areas as elements where the dislocation is two times greater than the average. Our assumed fault size of 46 km is almost the same as that in the 1995 Hyogo-ken Nanbu earthquake, and this event exhibited 2 or 3 asperity areas. We also assume an asperity distribution for this 46 km model. The width of our model is assumed to be 18 km, because the depth of the Conrad discontinuity is 20 km around the site. From Somerville et al. (1993), the asperity area is approximately 26% of the total rupture area, so the asperity in this case is about 215 km^2. Further, Somerville et al. (1993) determined empirical relations between rupture area, seismic moment, and dislocation. From these relations, the moment, average dislocation, and asperity dislocation are estimated to be 2.57×10^{26}dyne*cm,

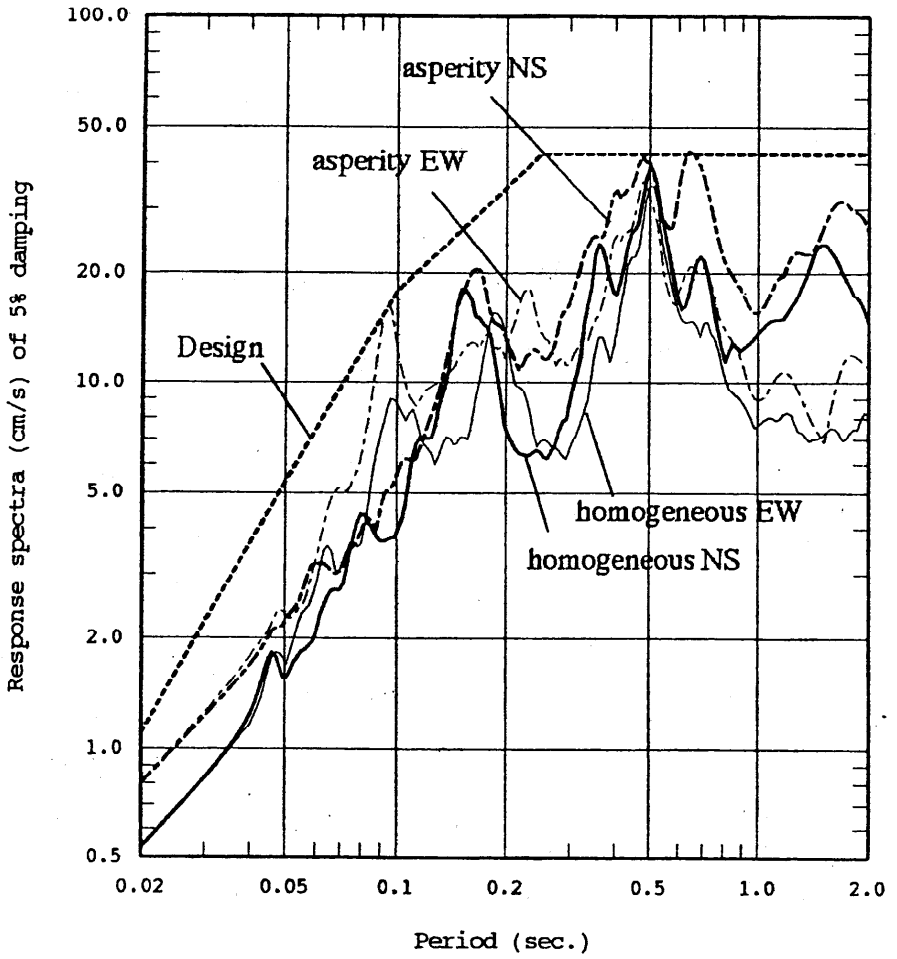

Figure 7. Pseudo velocity response spectra of 5% damping for 46 km homogeneous and asperity models, and design spectra.

99 cm, and 191 cm, respectively. Asperities are likely to occur near segmentation boundaries, so we place asperity areas on both sides of the fault model and another at the eastern end of the Iyonada fault group, all with a depth of 6km. Each asperity is 9 × 9 km^2. The total area of the three asperities is close to 26% of the rupture area. The moment for an asperity area is:

$$Mo = \mu LWD = 3 \times 4.0 \times 10^{11} \text{ dyne/cm}^2 \times 81 \text{ km}^2 \times 191 \text{ cm} = 1.86 \times 10^{26} \text{dyne*cm} \quad (2)$$

The general scaling is described by equation (1), though the dislocation of asperity D_A is twice as large. Namely:

$$D_A/D_S = 2D_L/D_S = 2n \quad (3)$$

Therefore, the ratio of small event moment to asperity moment, Mo_A, is

$$Mo_A/Mo_S = 2n^3 \quad (4)$$

If we take n = 3, the moment of the small event is 1.15 × 10^{24} dyne*cm, which is little different from the 1.52 × 10^{24} dyne*cm of the middle-sized event. Namely, the n for dislocation, length, and width of this event is 6, 3, and 3. As shown in Figure 1, small elements are arranged, totalling 15 for the length and 6 for the width. The stress drop may be proportional to the dislocation, so 100 bar is assumed for the asperity area. The dislocation for non asperity areas is 30cm because the total moment must evaluate to 2.57 × 10^{26}dyne*cm. And the stress drop is 15 bar due to the proportionality with dislocation. The rupture initiation point is the deepest point at the eastern end.

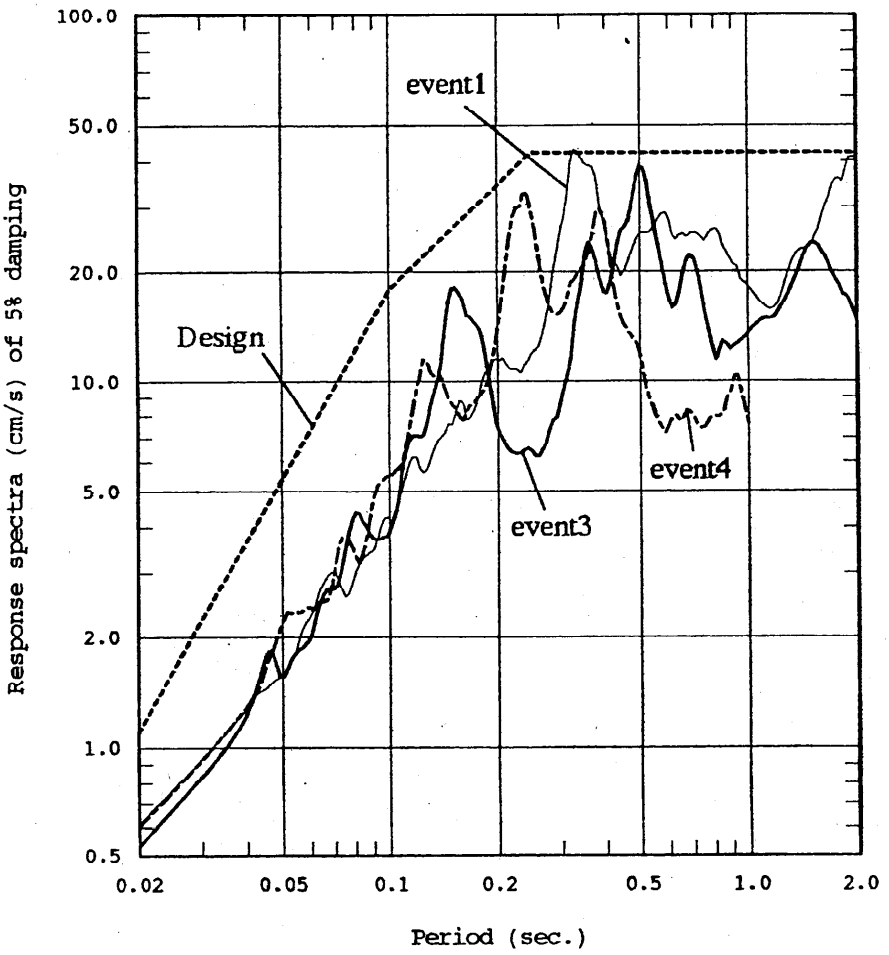

Figure 8. Pseudo velocity response spectra of 5% damping for model length of 46 km, and design spectrum. Green's functions are NS component of events 1, 3 and 4.

Results

Waveform

On the basis of event 3, the synthesized waveforms for the 27, 46, 55, and 77 km models, as well as the results for the asperity model, are shown in Figure 5. Duration rises with fault length. Three clear phases can be seen in the waveform of the asperity model. As shown in Table 2, the peak amplitude of the asperity model is the largest, and about 250 cm/s^2. This may be due to the high stress drop of the asperity. Although records from the other events are not appropriate as Green's functions, synthesized waves are also derived for the homogeneous model of 46 km for comparison purposes.

Pseudo Response Spectra of 5% damping

The pseudo velocity response, which is the divided spectral acceleration by ω, are calculated for 5% damping. The velocity response spectra for the NS component are shown in Figure 6 for the individual fault length models with a design basis spectrum of the plant. Even as the fault length increases, the responses do not vary much. This indicates that the nearest element effected to the level, because the source size does not effect to the spectra of this predominant period range and expected to be the distance is more effective than the size. The response spectra for the 46 km homogeneous and asperity models are shown in Figure 7. The dips at around 0.3 and 0.8 in the asperity model are shallower than those in the homogeneous model. The response spectra in the case of events 1, 3, and 4

are shown for homogeneous model in Figure 8. The dispersion is large, but each spectrum is smaller than the design spectrum.

Conclusion

Response spectra for all the synthesized waveforms are smaller than the design spectra, and although many rough assumptions are made for parameters with uncertain values, there are no significant differences in the estimated ground motions for the individual fault lengths. This indicates that the effect of source size is relatively small for strong ground motion of short period due to the random summation of the high-frequency phase. For the same reason and the azimuthal variety, directivity may less affect the high-frequency component. Aki (1968) also noted that the fault length and depth have a negligible effect on short-period ground motion. The JMA (Japan Meteorological Agency) intensity in the near-fault region is presented for a number of past earthquakes, and it appears to be independent of source size. Namely, intensity VII was first introduced after the 1948 Fukui earthquake of M_J 7.1 and was next experienced in the 1995 Hyogo-ken Nanbu earthquake of M_J 7.2, but the intensity during larger events (for example the 1891 Nobi earthquake of M_J 8.0 and the 1923 Great Kanto earthquake) reached only VI, although intensity VII had not yet been defined in 1891 and most part of fault traces in the 1923 Great Kanto earthquake were located offshore. Only the dips in the spectrum for the asperity model are shallower than those of the homogeneous model. This may be due to inhomogeneity and the inclusion of various frequency components in the synthesized waveform. Namely, the spectrum shape of Green's function from the asperity is different from the non-asperity elements. Therefore various frequency components are contained in the synthesized waveform for the asperity model than the homogeneous models.

Acknowledgement

We acknowledge with gratitude the valuable help provided by Prof. K. Irikura of the Disaster Prevention Research Institute, Kyoto University. Dr K. Dan offered his code and kind comments. Further, comments of anonymous reviewers improved this manuscript.

References

Aki, K., 1968, Seismic displacements near a fault, *J. Geophys. Res.* **73**, 5359–5376.

Brune, J., 1970, Tectonic stress and the spectra of seismic shear waves from earthquakes, *J. Geophys. Res.* **75**, 4997–5009.

Bour, M. and Cara, M., 1997, Test of a simple empirical Green's function method on moderate-sized earthquakes, *Bull. Seism. Soc. Am.* **87**, 668–683.

Dan, K., Tanaka, T. and Watanabe, T., 1987, Simulation and prediction of strong ground motion in epicentral region of the 1979 Imperial valley earthquake by seimi-empirical method, *J. Struct. Constr. Eng., AIJ* **373**, 50–62.

Dan, K., Watanabe, T. and Tanaka, T., 1990a, Stability of earthquake ground motion synthesized by using different small-event records as empirical Green's functions, *Bull. Seism. Soc. Am.* **80**, 1433–1455.

Dan, K., Watanabe, T. and Tanaka, T., 1990b, Estimation of strong ground motion in epicentral region of the 1976 Tangshan, China, earthquake (Ms7.8) by semi-empirical method, *J. Struct. Constr. Eng., AIJ* **407**, 23–33.

Dan, K., Ishii, T. and Ebihara, M., 1993, Estimation of strong ground motions in meizoseismal region of the 1976 Tangshan, China, earthquake, *Bull. Seism. Soc. Am.* **83**, 1756–1777.

Dan, K. and Sato, T., 1998, Simulation of strong ground motions in the near field of the 1979 Imperial valley, California, earthquake by seimi-empirical method based on variable-slip rupture model, *Proc. 10th Japan Earthq. Eng. Symposium* 703–708.

Dieterich, J.H., 1973, A deterministic near-field source model, *Proc. 5th World Conf. on Earthq. Eng.* **2**, 2385–2396.

Kamae K. and Irikura, K., 1998, Source model of the 1995 Hyogo-ken Nanbu earthquake and simulation of near-source ground motion, *Bull. Seism. Soc. Am.* **88**, 400–412.

Kobayashi, H. and Midorikawa, S., 1982, A semi-empirical method for estimating response spectra of near-field ground motions with regard to fault rupture, *Proc. 7th European Conf. on Earthq. Eng.* 161–168.

Liu, H.L. and Helmberger, D., 1985, The 23:19 aftershock of the 15 October 10979 Imperial valley earthquake: More evidence for an asperity, *Bull. Seism. Soc. Am.* 75, 689–708.

Matsuda, T., 1975, Magnitude and recurrence interval of earthquake from a fault, *Zishin* **2, (28)** 269–283. (in Japanese)

Ohno Y., Kobayashi, S. and Hasegawa, S., 1998, Determination of design basis earthquakes from active faults, *8th International IAEG Congress* 837–844.

Sato, R., 1989, Fault parameter handbook in Japan, Kajima-shuppankai, Tokyo. (in Japanese)

Somerville P.G., Sen, M., and Cohee, B., 1991, Simulation of strong ground motions recorded during the 1985 Michoacan, Mexico and Valparaiso, Chile earthquakes, *Bull. Seism. Soc. Am.* **81**, 1–27.

Somerville P.G., Irikura, K., Sawada, S., Iwasaki, Y., Tai, Y. and Fushimi, M., 1993, A study of slip distribution in earthquake fault, *Proc. 23 JSCE Earthq. Eng. Sympo., Japan Soc. Civil Eng.* 291–294. (in Japanese)

Wald, D.J., 1996. Slip history of the 1995 Kobe, Japan, earthquake determined from strong motion, teleseismic, and geodetic data, *J. Phys. Earth* **44**, 489–503.

Zhao, W., Dan, K. and Tanaka, T., 1995, Scaling factors in different semi-empirical methods for synthesizing earthquake motions, *J. Struct. Constr. Eng., AIJ* **471**, 29–40. (in Japanese)

Zhao, W., Dan, K. and Tanaka, T., 1996, The authors' answers to the discussion by Dr Tomonori Ikeura and Dr Masayuki Takemura, *J. Struct. Constr. Eng., AIJ* **480**, 187–188. (in Japanese)